RESEARCH ARTICLE

Carbon Fiber Supported Binary Metal Sulfide Catalysts with Multi-Dimensional Structures for Electrocatalytic Nitrogen Reduction Reactions Over a Wide pH Range

Tianyi Zhang[1] · Wei Zong[1] · Yue Ouyang[1] · Yue Wu[2] · Yue-E Miao[1] · Tianxi Liu[1,3]

Abstract

Green and environmentally friendly electrocatalytic nitrogen (N_2) fixation to synthesize ammonia (NH_3) is recognized as an effective method to replace the traditional Haber–Bosch process. However, the difficulties in N_2 adsorption and fracture of hard N≡N bond still remain major challenges in electrocatalytic N_2 reduction reactions (NRR). From the perspectives of enhancing N_2 adsorption and providing more catalytic sites, two-dimensional (2D) FeS_2 nanosheets and three-dimensional (3D) metal organic framework-derived ZnS embedded within N-doped carbon polyhedras are grown on the carbon cloth (CC) template in this work. Thus, a composite NRR catalyst with multi-dimensional structures, which is signed as FeS_2/ZnS-NC@CC, is obtained for using over a wide pH range. The uniform distribution of hollow ZnS-NC frameworks and FeS_2 nanosheets on the surface of CC largely increase the N_2 enrichment efficiency and offer more active sites, while the CC skeleton acts as an independent conductive substrate and S-doping helps promote the fracture of N≡N bond during the NRR reaction. As a result, the FeS_2/ZnS-NC@CC electrode achieves a high Faraday efficiency of 46.84% and NH_3 yield of 58.52 μg h^{-1} mg^{-1} at -0.5 V vs. Ag/AgCl in 0.1 M KOH. Furthermore, the FeS_2/ZnS-NC@CC electrode displays excellent NRR catalytic activity in acidic and neutral electrolytes as well, which outperforms most previously reported electrocatalysts including noble metals. Therefore, this work provides a new way for the design of multi-dimensional electrocatalysts with excellent electrocatalytic efficiency and stability for NRR applications.

Keywords Multi-dimensional structure · Heteroatom doping · Carbon fiber cloth · Electrocatalytic nitrogen reduction

Introduction

Known as one of the most important fertilizer feedstocks and energy carriers in the twenty-first century, ammonia (NH_3) is widely used in agriculture and industry fields [1–3]. Industrially, the production of NH_3 mainly uses the highly efficient Haber–Bosch process [4]. Unfortunately, the energy-intensive process is carried out under harsh conditions and causes abundant greenhouse gas emission which puts great burden on the environment [5–8]. Therefore, to alleviate these conditions, the exploration of a green and sustainable method for nitrogen (N_2) fixation has drawn tremendous interests. Electrocatalytic N_2 reduction reaction (NRR) can directly use the electricity generated by renewable energy sources to convert N_2 and H_2O into NH_3, and guarantee zero emission of carbon dioxide [9, 10]. Nevertheless, the environmentally-friendly NRR technique has encountered performance obstacles, such as the difficult adsorption of N_2, competitive hydrogen evolution reaction (HER) process and stable N≡N

✉ Yue Wu
  wuyue@dhu.edu.cn

✉ Yue-E Miao
  yuee_miao@dhu.edu.cn

1 State Key Laboratory for Modification of Chemical Fibers and Polymer Materials, College of Materials Science and Engineering, Innovation Center for Textile Science and Technology, Donghua University, 2999 North Renmin Road, Shanghai 201620, People's Republic of China

2 Research Center for Analysis and Measurement, Donghua University, Shanghai 201620, People's Republic of China

3 Key Laboratory of Synthetic and Biological Colloids, Ministry of Education, School of Chemical and Material Engineering, Jiangnan University, Wuxi 214122, People's Republic of China

bond, resulting in the low NH_3 yield and Faraday efficiency (FE) [11–13]. Therefore, to design and synthesize highly effective, easily available and durable heterogeneous electrocatalysts is still extremely challenging [14–17].

To design high-performance NRR catalyst, researchers mainly proceed from the following two aspects. On the one hand, from the perspective of biological N_2 fixation in nature, nitrogenase containing Fe, Mo and S elements can selectively destroy the non-polar triple bond of N_2 [18, 19]. Transition metals are widely used as the main components of NRR catalyst due to their unique d-orbital electron arrangement and inexpensive characteristics [20]. In transition metals, the unoccupied d-orbital can receive the lone pair electrons of N_2 while the occupied d-orbital electrons can be fed back to the anti-bond orbital of N_2 [21, 22], thus leading to the effective interactions between the transition metals and N_2 [23]. Besides, the doping of S atoms can improve the physical and chemical adsorption capacity of the catalyst for N_2, thereby enhancing the catalytic performance of NRR [24]. Therefore, inspired by the biological N_2 fixation and electronic arrangement of transition metals, various NRR catalysts based on transition metal sulfides, such as MoS_2 [8], FeS_2 [25], NiCoS [26] and FeMoS [27], have received extensive attentions for their excellent N_2 reduction performance. For example, Sun et al. have reported a composite catalyst of carbon fiber cloth (CFC) covered with FeS dotted MoS_2 nanosheet [27]. Due to its good morphological controllability, the composite catalyst demonstrates an electrochemical ammonia synthesis rate of 8.45 μg h^{-1} cm^{-1} and a FE of 2.96% at -0.5 V vs. RHE in the neutral pH electrolyte. On the other hand, starting from the structural design of the catalyst, two-dimensional (2D) nanomaterials have attracted much attention in the field of catalysis due to their high specific surface area [28, 29]. However, agglomeration and stacking tend to occur during the reaction process, leading to the inactivation of the catalytic sites. Therefore, the construction of multi-dimensional structures by the combination of 2D nanomaterials with other nanostructures is considered as an effective strategy to increase the space between 2D nanomaterials to avoid agglomeration and improve the exposure of active sites [30].

It is well known that metal organic frameworks (MOFs) formed by bridging metal ions and organic linkers have gradually become a new type of crystalline material [31–33]. With high structural stability, large specific surface area and abundant pores, the 3D MOF skeleton can inherit its original highly porous nanostructure and other excellent properties after heat treatment [34, 35]. These characteristics can guarantee the fast mass transfer, large gas enrichment and rich potential active sites for MOF-derivatives, which makes them potential candidates to improve the electrocatalytic NRR activity [36–38]. However, there are still some problems such as poor conductivity and easy agglomeration

problems in directly using MOF-derivatives as NRR electrocatalyst [39]. Therefore, how to promote the uniform dispersion and conductivity of MOF derivatives is a key issue to ensure the full exposure of the active sites and rapid electron transport without agglomeration of the catalyst [40].

The commercial carbon cloth (CC) is consisting of carbon fibers, which possess the advantages of excellent electrical conductivity and gas permeability. Herein, a flexible composite catalyst, which is composed of CC supported 2D FeS_2 nanosheets coupled with ZnS embedded within 3D N-doped carbon polyhedra (signed as FeS_2/ZnS-NC@CC), has been prepared for NRR applications. The CC substrate in the composite electrocatalyst acts as the conductive template to improve the electron transport of NRR, while the surface coating of 2D FeS_2 nanosheets and 3D ZnS-NC nanoislands forms a hierarchical architecture. Compared with traditional 2D and 3D structured catalysts, the design of the multidimensional structure is expected to ensure the rapid mass transfer, promote the N_2 enrichment ability and abundant potential active sites for improving the performance of electrocatalytic NRR. Furthermore, the self-supporting FeS_2/ZnS-NC@CC composite can be directly used as a cathode without additional binders and conductive additives. Besides, the close contact between the electrocatalytic components and the flexible CC substrate can effectively avoid the severe agglomeration and shedding of the traditional powdery catalyst, being beneficial to enhancing the stability of the catalyst. As a result, the FeS_2/ZnS-NC@CC composite cathode exhibits excellent NRR catalytic performance over a wide pH range, especially with a high NH_3 yield of 58.52 μg h^{-1} mg^{-1} and FE of 46.84% at -0.5 V vs. Ag/AgCl using 0.1 M KOH electrolyte. Meanwhile, the catalyst displays outstanding catalytic stability in alkaline and neutral electrolytes as well, which shows a good prospect for designing highly efficient and stable NRR catalysts.

Results and Discussion

Typically, a three-step synthetic route is adopted to fabricate the FeS_2/ZnS-NC@CC composite as shown in Fig. 1. First, ultra-thin Fe and Zn layered double hydroxide (FeZn-LDH) nanosheets are uniformly grown on the surface of CC by hydrothermal method to obtain FeZn-LDH@CC composite. Then, the as-prepared Zn-containing FeZn-LDH nanosheets are used as the metal source, and the in-situ phase structure is reconstructed by coordination with 2-methylimidazole (2-MeIM) under low temperature. Thus, CC-supported 2D Fe-LDH nanosheets co-existing with zeolitic imidazolate framework-8 (ZIF-8) dodecahedra precursors are achieved as Fe-ZIF-8@CC. Finally, the sublimation of sulfur is carried out to provide S source for vulcanization of Fe-ZIF-8@CC. Thus, the FeS_2/ZnS-NC@CC composite is obtained in

Fig. 1 Schematic illustration of the synthetic process of FeS$_2$/ZnS-NC@CC
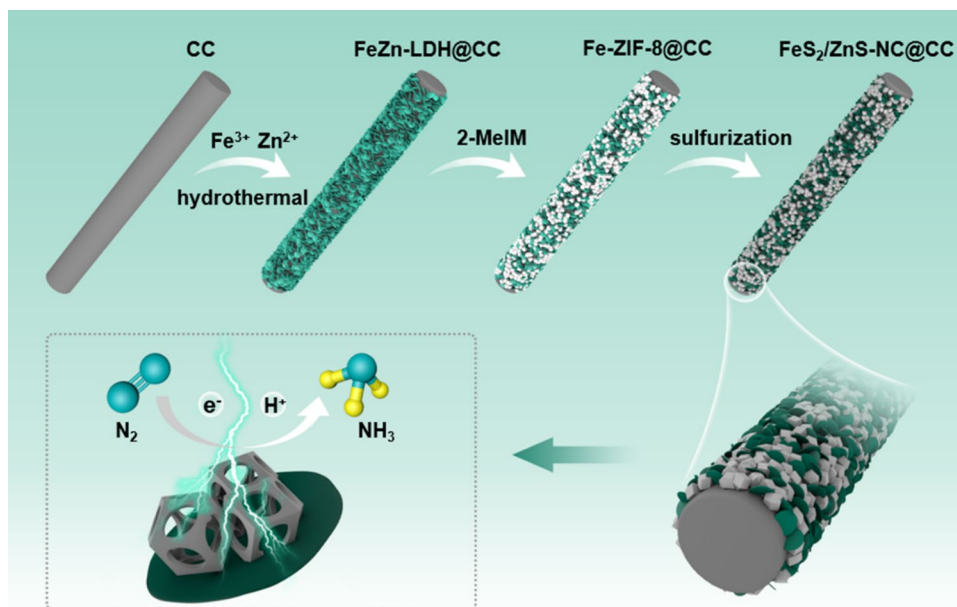

which 2D FeS$_2$ nanosheets and ZnS embedded within 3D N-doped carbon nanoislands are coexisting.

Scanning electron microscopy (SEM) images of FeZn-LDH@CC, Fe-ZIF-8@CC and FeS$_2$/ZnS-NC@CC are shown in Fig. 2. It can be observed that 2D FeZn-LDH nanosheets are uniformly distributed on the surface of carbon fibers (Fig. 2a, d). After the coordination reaction of FeZn-LDH@CC with 2-MeIM, ZIF-8 are formed in the SEM images of Fe-ZIF-8@CC (Fig. 2b, e), indicating the successful coordination of Zn species with the organic ligands. Meanwhile, the original ZIF-8 polyhedra architecture is converted into 3D hollow N-doped carbon

polyhedron loaded with ZnS after vulcanization, forming a unique multi-dimensional structure with the co-existence of 2D FeS$_2$ nanosheets and 3D ZnS-NC nanoislands in the FeS$_2$/ZnS-NC@CC composite (Fig. 2c, f, S1). The corresponding elemental mappings demonstrate that Fe, Zn, S and N elements are uniformly distributed on CC (Fig. 2g).

To further confirm the hierarchical structure, the FeS$_2$/ZnS-NC composite stripped from FeS$_2$/ZnS-NC@CC by ultrasonic method is tested by transmission electron microscopy (TEM). As shown in Fig. 3a, the coexistence of 2D nanosheets and 3D ZIF-8-derived nanocrystals can be observed after pyrolysis. For comparison, the TEM image

Fig. 2 SEM images of FeZn-LDH@CC (**a**, **d**), Fe-ZIF-8@CC (**b**, **e**) and FeS$_2$/ZnS-NC@CC (**c**, **f**); the corresponding EDX elemental mappings of Fe, Zn, S and N (**g**)
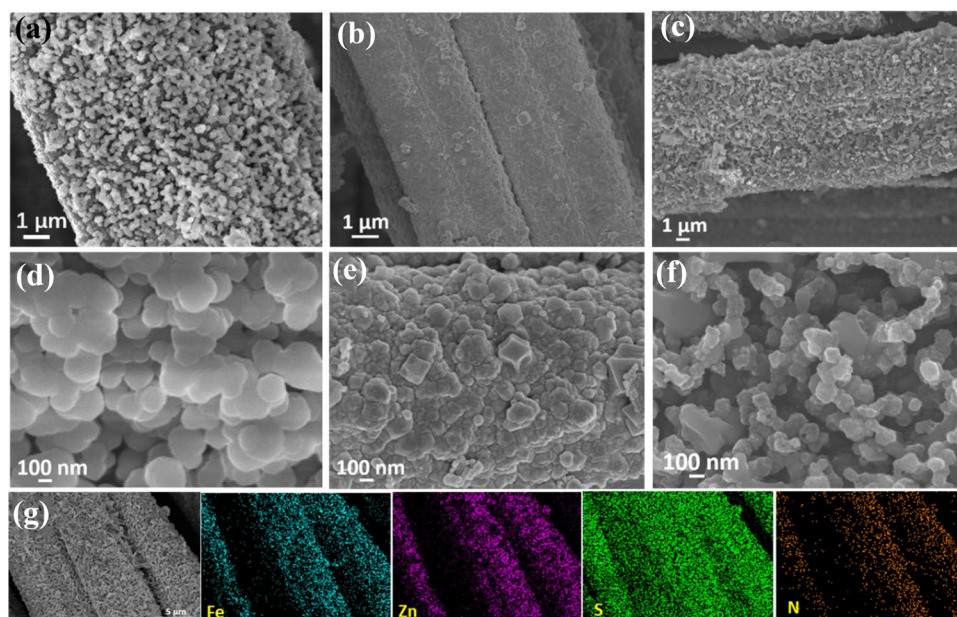
Fig. 3 **a** TEM and **b** HRTEM images of FeS$_2$/ZnS-NC; **c** XRD patterns of FeZn-LDH@CC, Fe-ZIF-8@CC and FeS$_2$/ZnS-NC@CC; **d** TGA of FeS$_2$/ZnS-NC@CC in air and N$_2$
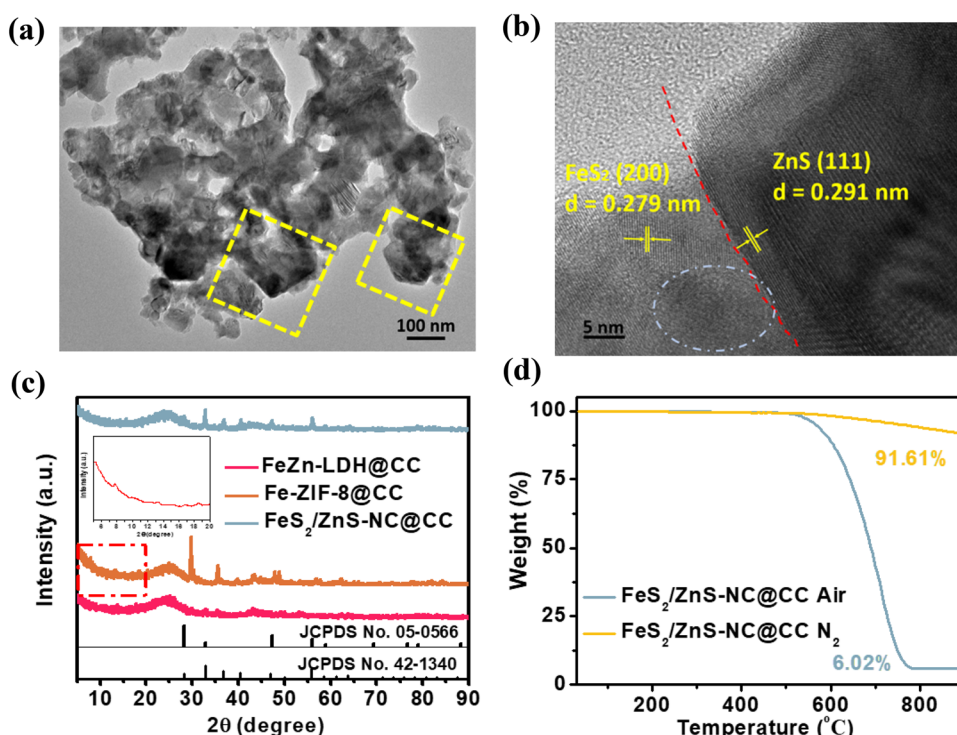
of FeZn-LDH is presented in Fig. S2, indicating an ultrathin layered nanosheet structure. Figure 3b displays the high-resolution TEM (HRTEM) image of FeS$_2$/ZnS-NC which shows the lattice fringes with spacing of 0.279 nm and 0.291 nm, corresponding to the (200) plane of FeS$_2$ [41] and the (111) plane of ZnS [42] respectively. In addition, the clear HRTEM interface marked by the red dashed line is due to the disordered structure caused by the mismatch between FeS$_2$ and ZnS phases [41]. In order to determine the phase transformation from FeZn-LDH@CC to FeS$_2$/ZnS-NC@CC, X-ray diffraction (XRD) patterns are obtained in Fig. 3c. The diffraction pattern of FeZn-LDH@CC shows peaks at $2\theta = 28.4°$, 35.6° and 63.6° which can be attributed to the (003), (110), and (300) diffraction planes of Fe-LDH (JCPDS No. 46-1315). The peaks centered at $2\theta = 24.9°$, 33.0° and 42.8° are assigned to the (004), (105) and (314) of Zn-LDH (JCPDS No. 38-0356) respectively, indicating that FeZn-LDH@CC is successfully prepared. Compared with FeZn-LDH@CC, the XRD pattern of Fe-ZIF-8@CC shows characteristic diffraction peaks at $2\theta = 7.4°$, 10.4°, 16.5° and 18.1°, which are consistent with the (101), (002), (013) and (222) of ZIF-8 [43, 44]. Nonetheless, the ZIF-8 diffractions disappear while the characteristic diffraction peaks of FeS$_2$ and ZnS appear after vulcanization, which strongly illustrate the formation of FeS$_2$/ZnS-NC@CC. In particular, the XRD pattern of FeS$_2$/ZnS-NC@CC shows characteristic peaks around $2\theta = 28.5°$, 33.0°, 37.1°, 40.7°, 47.4° and 50.5°, which are indexed to (111), (200), (210), (211), (220) and (221) diffractions of FeS$_2$ (JCPDS No.

42-1340). Meanwhile, the diffraction peaks at $2\theta = 47.5°$, 56.3° and 59.1° are corresponding to the (220), (311) and (222) crystal planes of ZnS (JCPDS No. 05-0566). Thermogravimetric (TGA) curves are acquired to analyze the Fe and Zn contents in FeS$_2$/ZnS-NC@CC (Fig. 3d). The content of Zn is calculated to be 8.19 wt% by the weight loss at 900 °C under N$_2$ atmosphere, while the mass ratio of ZnS is 12.2 wt%. Besides, the weight loss of FeS$_2$/ZnS-NC@CC composite reaches 93.98 wt% between 508 °C and 780 °C in air, which is caused by the oxidative decompositions of ZnS (500–620 °C) [45, 46] and CC (500–700 °C) [47, 48]. As the weight retention of the final product of Fe$_2$O$_3$ is 6.02 wt%, the mass ratio of FeS$_2$ in the composite is calculated to be 4.5 wt% according to the transformation of Fe$_2$O$_3$ to FeS$_2$ with a mass change of 133.3%.

The chemical structure and elemental composition of FeS$_2$/ZnS-NC@CC are further examined by X-ray photoelectron spectroscopy (XPS). As shown in Fig. 4a, the survey spectrum of XPS reveals the presences of Zn, Fe, S, N and C elements in the FeS$_2$/ZnS-NC@CC composite. The peaks located at 707.4 eV and 720.1 eV for Fe 2p$_{3/2}$ and Fe 2p$_{1/2}$ indicate the oxidation state of Fe^{2+} (Fig. 4b). For the high-resolution Zn 2p spectrum (Fig. 4c), two peaks at 1022.4 eV and 1045.5 eV, are assigned to the binding energies of Zn 2p$_{5/2}$ and Zn 2p$_{3/2}$, respectively. In the S 2p spectrum (Fig. 4d), the peaks at 162.8 eV and 163.9 eV belong to S 2p$_{3/2}$ and S 2p$_{1/2}$, while the other peaks are due to the presence of sulfur oxide species. The combined XPS data clearly demonstrate that the composite FeS$_2$/ZnS-NC@
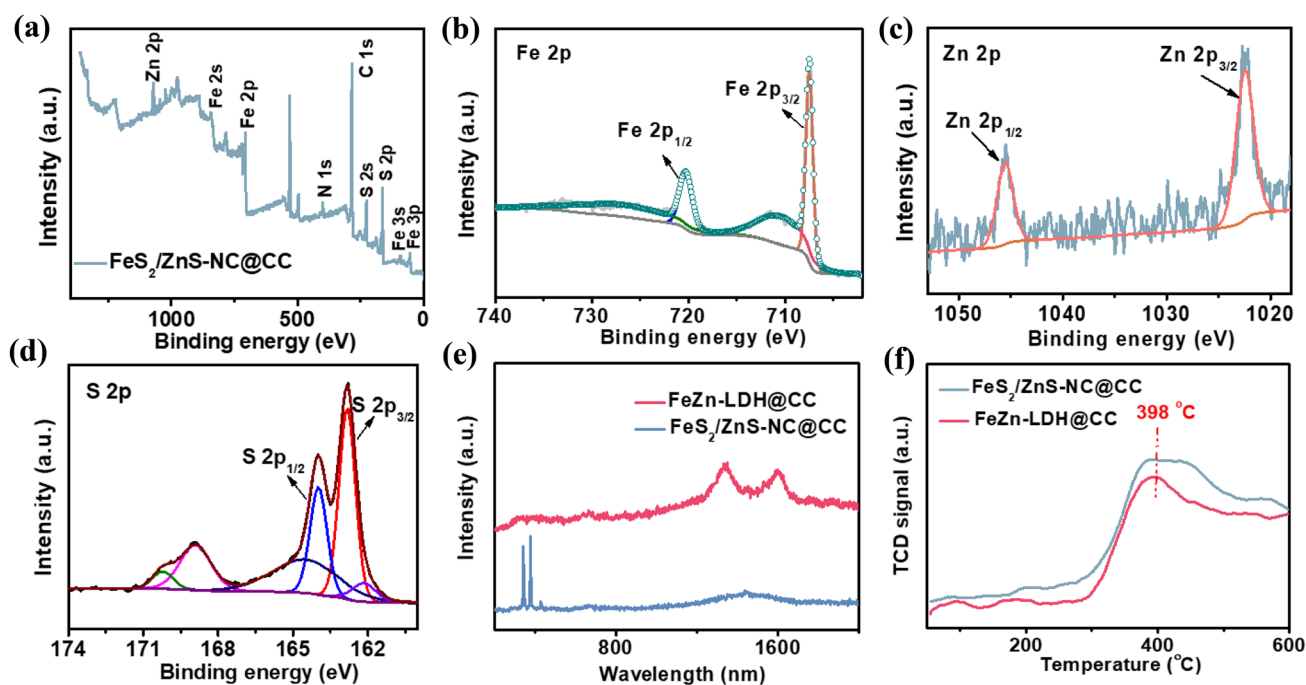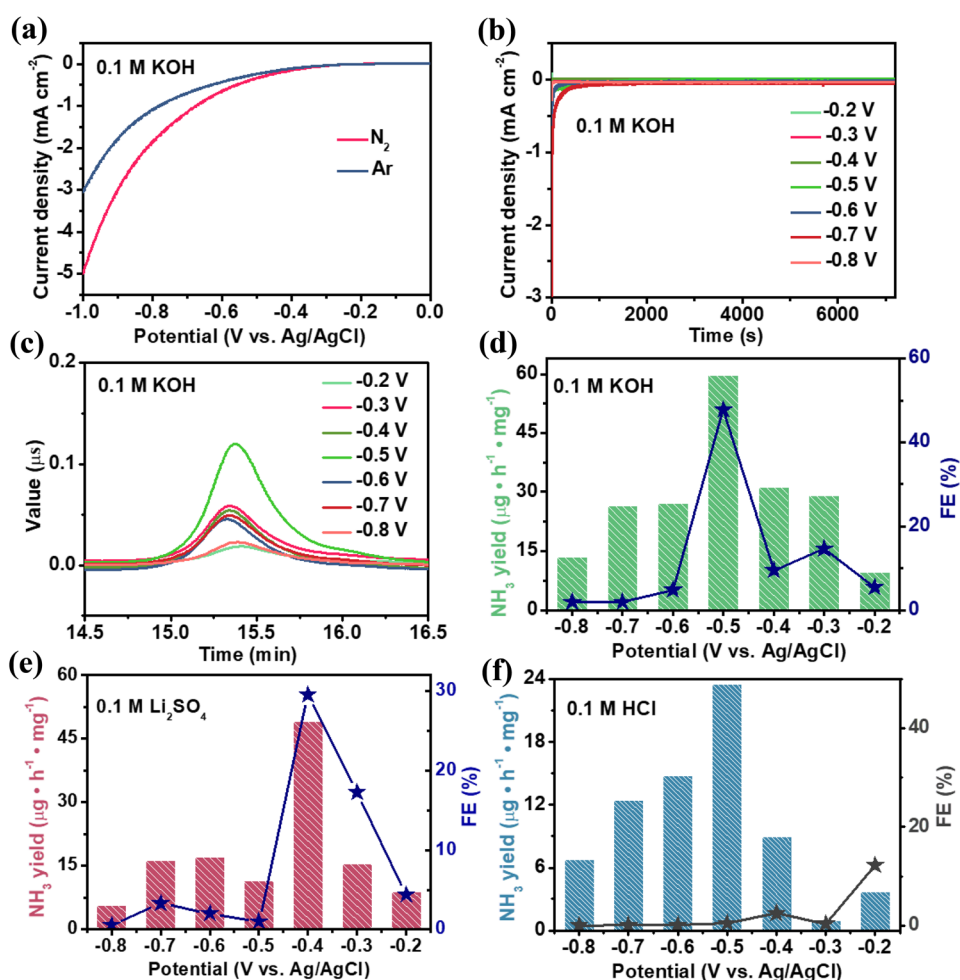
Fig. 4 **a** XPS survey spectrum of FeS$_2$/ZnS-NC@CC; and the corresponding high-resolution XPS spectra of **b** Fe 2p, **c** Zn 2p and **d** S 2p. **e** Raman spectra and **f** N$_2$-TPD spectra of FeZn-LDH@CC and FeS$_2$/ZnS-NC@CC

CC electrocatalyst is composed of FeS$_2$ and ZnS [41, 42]. Furthermore, Raman spectra of both FeZn-LDH@CC and FeS$_2$/ZnS-NC@CC are observed in Fig. 4e. Compared with FeZn-LDH@CC, FeS$_2$/ZnS-NC@CC shows characteristic peaks of the inorganic species below 1000 cm^{-1}. In detail, the two peaks at 343.6 cm^{-1} and 377.9 cm^{-1} represent the diffraction peaks of FeS$_2$, while the peaks at 420 cm^{-1} and 429.4 cm^{-1} can be assigned to ZnS, further verifying the formation of FeS$_2$ and ZnS [49]. Besides, the I_D/I_G value of FeS$_2$/ZnS-NC@CC increases after sulfurization, indicating the increased disorder structure of carbon material which can enhance the electrocatalytic activity. As the construction of hierarchical FeS$_2$/ZnS-NC structure is to improve the adsorption capacity of N$_2$ on the catalyst, the N$_2$ temperature programmed desorption (N$_2$-TPD) test is performed on FeZn-LDH@CC and FeS$_2$/ZnS-NC@CC. As shown in Fig. 4f, both of FeZn-LDH@CC and FeS$_2$/ZnS-NC@CC exhibit a peak at 398 °C, which is assigned to the chemical adsorption of N$_2$. Moreover, the TCD signal of FeS$_2$/ZnS-NC@CC with a multi-dimensional structure is higher than that of FeZn-LDH@CC, which verifies that ZnS nanoislands derived from ZIF-8 effectively promote the adsorption of N$_2$ and enhance the binding strength of N$_2$ on FeS$_2$/ZnS-NC@CC [26].

Ion chromatography is used to conduct quantitative analysis on the generated NH$_4^+$. Firstly, the linear relationship between the integral area and corresponding concentration is obtained by using the pre-configured standard solution

(Fig. S3). Then, the subsequent calculation is carried out according to this linear relationship. The NRR performance of FeZn-LDH@CC, Fe/Zn-NC@CC and FeS$_2$/ZnS-NC@CC is evaluated in 0.1 M KOH at − 0.5 V vs. Ag/AgCl. The corresponding NH$_3$ yield rate and FEs are calculated according to the linear relationship and ion chromatogram of the reaction electrolyte (Fig. S4a). Fig. S4b shows that the catalytic performance of FeS$_2$/ZnS-NC@CC is significantly higher than those of other two samples. Compared with FeZn-LDH@CC, the FeS$_2$/ZnS-NC@CC composite with a multi-dimensional structure is more conducive to the enrichment of N$_2$ toward the catalyst and increases the probability of N$_2$ attaching to the catalytic sites. However, the Fe/Zn-NC@CC composite without sulfurization shows inferior performance, indicating that sulfur-doping plays an indispensable role in improving the catalytic performance of FeS$_2$/ZnS-NC@CC. Then, linear sweep voltammetry (LSV) is carried out on the best performing FeS$_2$/ZnS-NC@CC composite. As displayed in Fig. 5a, when the voltage is less than -0.5 V vs. Ag/AgCl, the current density in 0.1 M KOH solution saturated with N$_2$ is slightly larger than that with Ar, indicating that FeS$_2$/ZnS-NC@CC has a high NRR catalytic activity. As illustrated in Fig. 5b, Time-dependent current density curves also show that the current density of FeS$_2$/ZnS-NC@CC remains unchanged for 2 h at different potentials, indicating the superior stability of the catalyst. The average NH$_3$ yield rates and corresponding FEs of FeS$_2$/ZnS-NC@CC under various applied potentials are

displayed in Fig. 5c, d, revealing a maximum integral area at -0.5 V vs. Ag/AgCl. The NH_3 yield and FEs can reach 58.52 µg h^{-1} mg^{-1} and 46.84% respectively, which exceed most previously reported NRR electrocatalysts under room temperature and pressure (Table S1).

In order to study the influence of the electrolyte on the catalyst performance, the NRR performance of the catalysts are further evaluated in neutral electrolyte of 0.1 M Li_2SO_4 and acid electrolyte of 0.1 M HCl. First, the NRR properties of FeZn-LDH@CC, Fe/Zn-NC@CC and FeS_2/ZnS-NC@CC in 0.1 M Li_2SO_4 and 0.1 M HCl are tested. Fig. S5a and S5b show that the unique structure and composition of FeS_2/ZnS-NC@CC catalyst have the best NRR performance. The time-dependent current density curves of FeS_2/ZnS-NC@CC show the same durability under long-term electrolysis in neutral and acid electrolytes (Fig. S5c and S5d). Meanwhile, the NRR performance of FeS_2/ZnS-NC@CC under different voltages in neutral and acid electrolytes are very similar to the electrolysis in KOH (Fig. 5e, f). In detail, the average NH_3 yield of FeS_2/ZnS-NC@CC can reach the highest value of 49.05 µg h^{-1} mg^{-1} with a FE of 29.5% at -0.4 V vs. Ag/AgCl in 0.1 M Li_2SO_4, while the highest average NH_3 yield

is only 23.52 µg h^{-1} mg^{-1} with significantly decreased FEs value in 0.1 M HCl. This is mainly due to the high concentration of H$^+$ in the acidic environment, which enhances the competitiveness of HER process and results in a significant reduction in NH_3 production. Comparisons of the performance of FeS_2/ZnS-NC@CC over a wide pH range indicates that the average NH_3 yield and FEs reach the maximum in alkaline electrolyte, which can be attributed to the prohibited HER process for the difficulty in breaking the strong hydrogen bonding in water molecules under alkaline environment. Furthermore, previous studies have proved that K$^+$ can effectively stabilize the N_2 reduction intermediates and regulate proton transfer, thus preventing hydrogen ions or protons from adsorbing on the active sites of the catalyst surface and suppressing the formation of hydrogen [50].

The possible by-product hydrazine hydrate (N_2H_4) during NRR is tested by the Watt–Chrisp method using UV–Vis spectrophotometer at 455 nm with the calibration curves of N_2H_4 shown in Fig. S6. According to the test curves in Fig. S7, FeS_2/ZnS-NC@CC presents excellent selectivity almost without N_2H_4 production. To further verify the remarkable catalytic performance of FeS_2/

ZnS-NC@CC toward high yield of NH$_3$, control experiments under different conditions are also performed (Fig. S8). Obviously, no NH$_4^+$ formation is detected at the open circuit potential, while the bare CC has no activity for NRR. Similarly, when pure water is used as electrolyte, no NH$_3$ is generated. When N$_2$ is replaced by Ar as the purge gas, no significant NH$_4^+$ product is examined, which solidly confirms that NH$_3$ is mainly produced by the reaction of N$_2$ with water, rather than by the autolysis of the catalyst. Proton nuclear magnetic resonance (^{1}H NMR) spectroscopy is also performed to further verify the formation of NH$_3$. As shown in Fig. S9, the standard peaks of NH$_4^+$ are observed in the ^{1}H NMR spectrum of the catalyzed electrolyte when ^{14}N$_2$ is used as the feeding gas, which proves the importance of N$_2$ in the NRR process.

Stability is another important criterion for evaluating catalysts in practical applications. Hence, the FeS$_2$/ZnS-NC@CC electrode is continuously running at the applied voltage of − 0.5 V vs. Ag/AgCl for 10 h in 0.1 M KOH. Figure 6a shows no significant change in current density while no obvious attenuation is observed in yield as shown in Fig. 6b, which reveal the high stability of FeS$_2$/ZnS-NC@CC in alkaline electrolyte. The same results also appear in the stability test of the neutral electrolyte (Fig. 6c, d). In strong contrast, the current density decreases significantly after continuous electrolysis for 2 h due to rich hydrogen ion concentration in acidic environment and metal sulfides exhibit poor structural stability under acidic conditions, thus

resulting in poor performance stability of FeS$_2$/ZnS-NC@CC electrode in 0.1 M HCl electrolyte (Fig. 6e, f).

Conclusions

As mentioned above, a multi-dimensional structure of FeS$_2$/ZnS-NC supported on the CC skeleton has been reported as a new-type of self-assembled electrode for electrochemical nitrogen reduction. Attributing to the precise morphological tuning, the FeS$_2$/ZnS-NC@CC composite can provide relatively uniform distribution of FeS$_2$ nanosheets and ZnS-NC nanoislands, which effectively improves the adsorption capacity of N$_2$, accelerates charge transfer and avoids agglomeration of 2D nanosheets. Moreover, the introduction of S enhances the ability of the catalyst to weaken N≡N bond, thereby improving the NRR performance. As a result, the obtained FeS$_2$/ZnS-NC@CC catalyst achieves the highest NH$_3$ yield of 58.52 µg h^{-1} mg^{-1} and FE of 46.84% at the potential of -0.5 V vs. Ag/AgCl in 0.1 M KOH. Meanwhile, the NRR results under acidic and neutral environments reveal that FeS$_2$/ZnS-NC@CC also shows excellent NRR performance over a wide pH range. Although the accompanying HER cannot be avoided in aqueous electrolyte, the NRR performance of the non-noble metal FeS$_2$/ZnS-NC@CC electrode under environmental conditions is superior to those of many previously reported catalysts. This work provides a novel idea for the design of NRR electrocatalysts
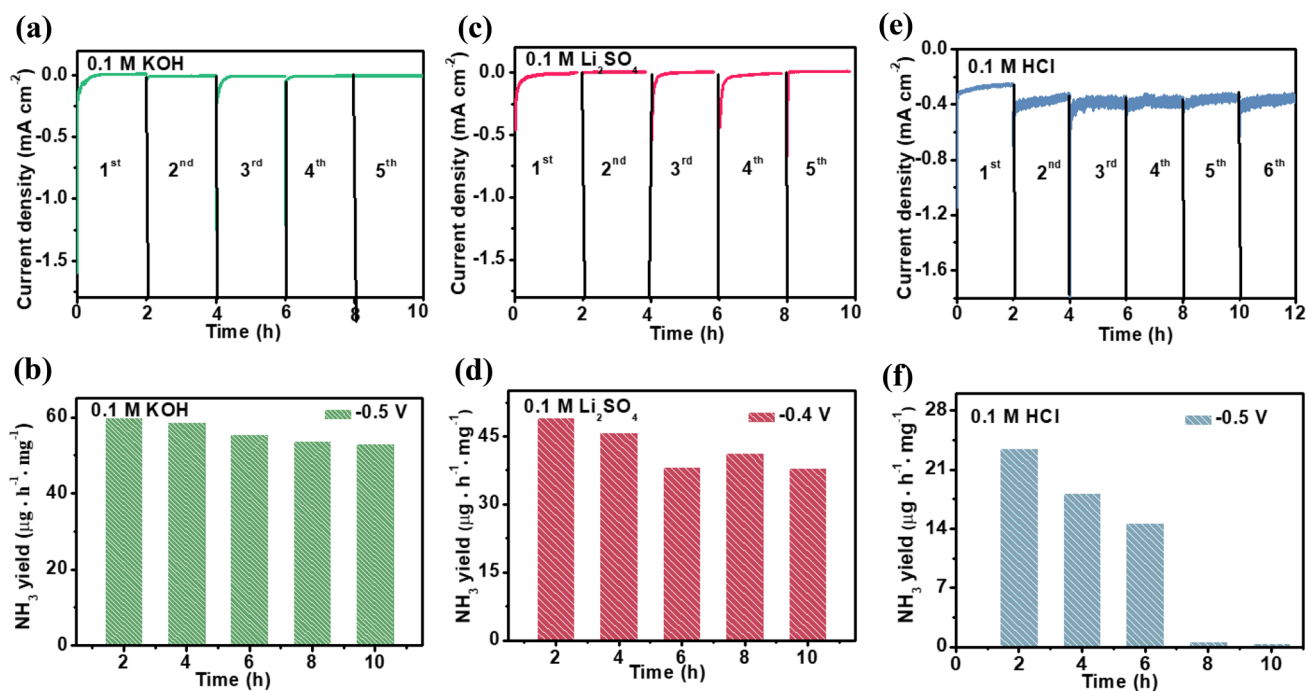
Fig. 6 Time-dependent current density cycle curves and average NH$_3$ yield cycle of FeS$_2$/ZnS-NC@CC electrode based on every 2 h electrolysis cycle under different pH electrolytes: **a**, **b** 0.1 M KOH; **c**, **d** 0.1 M Li$_2$SO$_4$; **e**, **f** 0.1 M HCl

with different components and structures to build up better artificial N_2 fixation systems under ambient conditions.

Compliance with Ethical Standards

Conflict of interest The authors declare no competing financial interest.

References

1. Service RF. New recipe produces ammonia from air, water, and sunlight. *Science.* **2014**;*345*:610.
2. Rosca V, Duca M, de Groot MT, Koper MTM. Nitrogen cycle electrocatalysis. *Chem Rev.* **2009**;*109*:2209–44.
3. Burgess BK, Lowe DJ. Mechanism of molybdenum nitrogenase. *Chem Rev.* **1996**;*96*:2983–3011.
4. Erisman JW, Sutton MA, Galloway J, Klimont Z, Winiwarter W. How a century of ammonia synthesis changed the world. *Nat Geosci.* **2008**;*1*:636–9.
5. Shipman MA, Symes MD. Recent progress towards the electrosynthesis of ammonia from sustainable resources. *Catal Today.* **2017**;*286*:57–68.
6. van der Ham CJM, Koper MTM, Hetterscheid DGH. Challenges in reduction of dinitrogen by proton and electron transfer. *Chem Soc Rev.* **2014**;*43*:5183–91.
7. Chirik PJ. One electron at a time. *Nat Chem.* **2009**;*1*:520–2.
8. Zhang L, Ji X, Ren X, Ma Y, Shi X, Tian Z, Asiri AM, Chen L, Tang B, Sun X. Electrochemical ammonia synthesis via nitrogen reduction reaction on a MoS_2 catalyst: theoretical and experimental studies. *Adv Mater.* **2018**;*30*:1800191.
9. Banerjee A, Yuhas BD, Margulies EA, Zhang Y, Shim Y, Wasielewski MR, Kanatzidis MG. Photochemical nitrogen conversion to ammonia in ambient conditions with FeMoS-chalcogels. *J Am Chem Soc.* **2015**;*137*:2030–4.
10. Sun K, Moreno-Hernandez IA, Schmidt WC Jr, Zhou X, Crompton JC, Liu R, Saadi F, Chen Y, Papadantonakis KM, Lewis NS. A comparison of the chemical, optical and electrocatalytic properties of water-oxidation catalysts for use in integrated solar-fuel generators. *Energy Environ Sci.* **2017**;*10*:987–1002.
11. Pang F, Wang Z, Zhang K, He J, Zhang W, Guo C, Ding Y. Bimodal nanoporous Pd_3Cu_1 alloy with restrained hydrogen evolution for stable and high yield electrochemical nitrogen reduction. *Nano Energy.* **2019**;*58*:834–41.
12. Deng J, Iniguez JA, Liu C. Electrocatalytic nitrogen reduction at low temperature. *Joule.* **2018**;*2*:846–56.
13. Singh AR, Rohr BA, Schwalbe JA, Cargnello M, Chan K, Jaramillo TF, Chorkendorff I, Norskov JK. Electrochemical ammonia synthesis-the selectivity challenge. *ACS Catal.* **2017**;*7*:706–9.
14. Kordali V, Kyriacou G, Lambrou C. Electrochemical synthesis of ammonia at atmospheric pressure and low temperature in a solid polymer electrolyte cell. *Chem Commun.* **2000**;*17*:1673–4.
15. Giddey S, Badwal SPS, Kulkarni A. Review of electrochemical ammonia production technologies and materials. *Int J Hydrog Energy.* **2013**;*38*:14576–94.
16. Lan R, Irvine JTS, Tao S. Synthesis of ammonia directly from air and water at ambient temperature and pressure. *Sci Rep.* **2013**;*3*:1145.
17. Wang J, Yu L, Hu L, Chen G, Xin H, Feng X. Ambient ammonia synthesis via palladium-catalyzed electrohydrogenation of dinitrogen at low overpotential. *Nat Commun.* **2018**;*9*:1795.
18. Cui X, Tang C, Zhang Q. A review of electrocatalytic reduction of dinitrogen to ammonia under ambient conditions. *Adv Energy Mater.* **2018**;*8*:1800369.
19. Eady RR. Structure–function relationships of alternative nitrogenases. *Chem Rev.* **1996**;*96*:3013–30.
20. Cao X, De J, Pan K. Electrospinning Janus type CoO_x/C nanofibers as electrocatalysts for oxygen reduction reaction. *Adv Fiber Mater.* **2020**;*2*:85–92.
21. Yandulov DV, Schrock RR. Catalytic reduction of dinitrogen to ammonia at a single molybdenum center. *Science.* **2003**;*301*:76–8.
22. Liu C, Li Q, Zhang J, Jin Y, MacFarlane DR, Sun C. Conversion of dinitrogen to ammonia on Ru atoms supported on boron sheets: a DFT study. *J Mater Chem A.* **2019**;*7*:4771–6.
23. Ling C, Niu X, Li Q, Du A, Wang J. Metal-free single atom catalyst for N_2 fixation driven by visible light. *J Am Chem Soc.* **2018**;*140*:14161–8.
24. Xia L, Wu X, Wang Y, Niu Z, Liu Q, Li T, Shi X, Asiri AM, Sun X. S-doped carbon nanospheres: an efficient electrocatalyst toward artificial N_2 fixation to NH_3. *Small Methods.* **2019**;*3*:1800251.
25. Sultana S, Mansingh S, Parida KM. Phosphide protected FeS_2 anchored oxygen defect oriented CeO_2NS based ternary hybrid for electrocatalytic and photocatalytic N_2 reduction to NH_3. *J Mater Chem A.* **2019**;*7*:9145–53.
26. Wu X, Wang Z, Han Y, Zhang D, Wang M, Li H, Zhao H, Pan Y, Lai J, Wang L. Chemically coupled NiCoS/C nanocages as efficient electrocatalysts for nitrogen reduction reactions. *J Mater Chem A.* **2020**;*8*:543–7.
27. Guo Y, Yao Z, Timmer BJJ, Sheng X, Fan L, Li Y, Zhang F, Sun L. Boosting nitrogen reduction reaction by bio-inspired FeMoS containing hybrid electrocatalyst over a wide pH range. *Nano Energy.* **2019**;*62*:282–8.
28. Ding Y, Chen YP, Zhang X, Chen L, Dong Z, Jiang HL, Xu H, Zhou HC. Controlled intercalation and chemical exfoliation of layered metal-organic frameworks using a chemically labile intercalating agent. *J Am Chem Soc.* **2017**;*139*:9136–9.
29. Chen S, Kang Z, Hu X, Zhang X, Wang H, Xie J, Zheng X, Yan W, Pan B, Xie Y. Delocalized spin states in 2D atomic layers realizing enhanced electrocatalytic oxygen evolution. *Adv Mater.* **2017**;*29*:1701687.
30. Zong W, Yang C, Mo L, Ouyang Y, Guo HL, Ge L, Miao YE, Rao D, Zhang J, Lai FL, Liu TX. Elucidating dual-defect mechanism in rhenium disulfide nanosheets with multi-dimensional ion transport channels for ultrafast sodium storage. *Nano Energy.* **2020**;*77*:150189.
31. Li J, Wang X, Zhao G, Chen C, Chai Z, Alsaedi A, Hayat T, Wang X. Metal-organic framework-based materials: superior adsorbents for the capture of toxic and radioactive metal ions. *Chem Soc Rev.* **2018**;*47*:2322–56.
32. Wu R, Wang DP, Rui X, Liu B, Zhou K, Law AWK, Yan Q, Wei J, Chen Z. In-situ formation of hollow hybrids composed of cobalt sulfides embedded within porous carbon polyhedra/carbon nanotubes for high-performance lithium-ion batteries. *Adv Mater.* **2015**;*27*:3038–44.
33. Chen Z, Wu R, Liu M, Wang H, Xu H, Guo Y, Song Y, Fang F, Yu X, Sun D. General synthesis of dual carbon-confined metal sulfides quantum dots toward high-performance anodes for sodium-ion batteries. *Adv Funct Mater.* **2017**;*27*:1702046.
34. Liu J, Zhu D, Guo C, Vasileff A, Qiao SZ. Design strategies toward advanced MOF-derived electrocatalysts for energy-conversion reactions. *Adv Energy Mater.* **2017**;*7*:1700518.

35. Li W, Shu R, Wu Y, Zhang J. Metal organic frameworks-derived iron carbide/ferroferric oxide/carbon/reduced graphene oxide nanocomposite with excellent electromagnetic wave absorption properties. *Compos Commun.* **2021**;*23*:100576.

36. Yu Z, Bai Y, Zhang S, Liu Y, Zhang N, Sun K. Metal-organic framework-derived $Zn_{0.975}Co_{0.025}S/CoS_2$ embedded in N,S-codoped carbon nanotube/nanopolyhedra as an efficient electrocatalyst for overall water splitting. *J Mater Chem A.* **2018**;*6*:10441–6.

37. Wu R, Wang DP, Zhou K, Srikanth N, Wei J, Chen Z. Porous cobalt phosphide/graphitic carbon polyhedral hybrid composites for efficient oxygen evolution reactions. *J Mater Chem A.* **2016**;*4*:13742–5.

38. Zhang J, Li Z, Yin G, Wang DY. Construction of a novel three-in-one biomass based intumescent fire retardant through phosphorus functionalized metal-organic framework and β-cyclodextrin hybrids in achieving fire safe epoxy. *Compos Commun.* **2020**;*23*:100594.

39. Wei J, Hu Y, Liang Y, Kong B, Kong B, Zhang J, Bao Q, Simon GP, Jiang SP, Wang H. Nitrogen-doped nanoporous carbon/graphene nano-sandwiches: synthesis and application for efficient oxygen reduction. *Adv Funct Mater.* **2015**;*25*:5768–77.

40. Guo J, Gao M, Nie J, Yin F, Ma G. ZIF-67/PAN-800 bifunctional electrocatalyst derived from electrospun fibers for efficient oxygen reduction and oxygen evolution reaction. *J Colloid Interface Sci.* **2019**;*544*:112–20.

41. Li Y, Yin J, An L, Lu M, Sun K, Zhao YQ, Gao D, Cheng F, Xi P. FeS_2/CoS_2 interface nanosheets as efficient bifunctional electrocatalyst for overall water splitting. *Small.* **2018**;*14*:1801070.

42. Huang L, Zhang Y, Shang C, Wang X, Zhou G, Ou JZ, Wang Y. ZnS nanotubes/carbon cloth as a reversible and high-capacity anode material for lithium-ion batteries. *Chemelectrochem.* **2019**;*6*:461–6.

43. Wang L, Fang M, Liu J, He J, Deng L, Li J, Lei J. The influence of dispersed phases on polyamide/ZIF-8 nanofiltration membranes for dye removal from water. *RSC Adv.* **2015**;*5*:50942–54.

44. Yoo J, Lee S, Lee CK, Kim C, Fujigaya T, Park HJ, Nakashima N, Shim JK. Homogeneous decoration of zeolitic imidazolate framework-8 (ZIF-8) with core-shell structures on carbon nanotubes. *RSC Adv.* **2014**;*4*:49614–9.

45. Mao M, Jiang L, Wu L, Zhang M, Wang T. The structure control of ZnS/graphene composites and their excellent properties for lithium-ion batteries. *J Mater Chem A.* **2015**;*3*:13384–9.

46. Fu Y, Zhang Z, Yang X, Gan Y, Chen W. ZnS nanoparticles embedded in porous carbon matrices as anode materials for lithium ion batteries. *RSC Adv.* **2015**;*5*:86941–4.

47. Wang H, Wang J, Cao D, Gu H, Li B, Lu X, Han X, Rogach AL, Niu C. Honeycomb-like carbon nanoflakes as a host for SnO_2 nanoparticles allowing enhanced lithium storage performance. *J Mater Chem A.* **2017**;*5*:6817–24.

48. Liu Y, Zhang N, Jiao L, Tao Z, Chen J. Ultrasmall Sn nanoparticles embedded in carbon as high-performance anode for sodium-ion batteries. *Adv Funct Mater.* **2015**;*25*:214–20.

49. Vázquez-Sánchez EE, Robledo-Cabrera A, Tong X, López-Valdivieso A. Raman spectroscopy characterization of some Cu, Fe and Zn sulfides and their relevant surface chemical species for flotation. *Physicochem Probl Miner Process.* **2020**;*56*:483–92.

50. Hao YC, Guo Y, Chen LW, Shu M, Wang XY, Bu TA, Gao W, Zhang N, Su X, Feng X, Zhou JW, Wang B, Hu CW, Yin AX, Si R, Zhang YW, Yan CH. Promoting nitrogen electroreduction to ammonia with bismuth nanocrystals and potassium cations in water. *Nat Catal.* **2019**;*2*:448–56.

Tianyi Zhang is a master student in College of Materials Science and Engineering, Donghua University. Her current research mainly focuses on the study of inorganic and metal composite material design and their electrocatalytic nitrogen reduction performance.

Wei Zong received his B.S. degree from Ludong University (2017). Now he is a Ph.D. candidate in College of Materials Science and Engineering, Donghua University. His current research interests include design and synthesis of advanced nanostructured materials for Li/Na/K-ion batteries and supercapacitors.

Yue Ouyang received her B.S. degree from Donghua University (2017). Now she is a Ph.D. candidate in College of Materials Science and Engineering, Donghua University. Her research focuses on design and preparation of high-performance carbon nanofiber composites in Li-S and Li-metal battery applications.

Yue Wu received her Master's degree in 2015 from Freiburg University in Germany. She is recently a senior lab technician in Donghua University. Her main research topics are devoted to (i) material surface morphology and composition analysis; (ii) develop new analytical methods and techniques for XPS and SEM.

Yue-E Miao received her B.S. degree from Southeast University in 2010 and Ph.D. degree from Fudan University in 2015. She is now an associate professor in College of Materials Science and Engineering, Donghua University. Her research interests mainly focus on high-performance organic fiber electrodes/separators, carbon nanofiber composites, as well as their applications in electrochemical energy storage devices (such as Li/Na-ion batteries and Li-S batteries).

Tianxi Liu obtained his BS degree from Henan University (1992) and Ph.D. degree from Changchun Institute of Applied Chemistry, Chinese Academy of Sciences (1998). He is currently a full professor in College of Materials Science and Engineering, Donghua University. His main research interests include polymer nanocomposites, organic/ inorganic hybrid materials, nanofibers and their composites, advanced energy materials for energy conversion and storage.